Tellus (2001), 53A, 168–191
Printed in UK. All rights reserved

TELLUS
ISSN 0280–6495

Downscaling of greenhouse gas induced climate change in two GCMs with the Rossby Centre regional climate model for northern Europe

By JOUNI RÄISÄNEN*, MARKKU RUMMUKAINEN and ANDERS ULLERSTIG,
Rossby Centre, Swedish Meteorological and Hydrological Institute, S-60176 Norrköping, Sweden

(Manuscript received 12 January 2000; in final form 24 October 2000)

ABSTRACT

Two 2×10-year climate change experiments made with the Rossby Centre regional Atmospheric climate model (RCA) are reported. These two experiments are driven by boundary data from two global climate change simulations, one made with HadCM2 and the other with ECHAM4/OPYC3, in which the global mean warming is virtually the same, 2.6°C. The changes in mean temperature and precipitation show similarities (including broadly the same increase in temperature and in northern Europe a general increase in annual precipitation) as well as differences between the two RCA experiments. These changes are strongly governed by the driving GCM simulations. Even on the RCA grid box scale, the differences in change between RCA and the driving GCM are generally smaller than the differences between the two GCMs. Typically about a half of the local differences between the two RCA simulations are attributed to noise generated by internal variability, which also seems to explain a substantial part of the RCA–GCM differences particularly for precipitation change. RCA includes interactive model components for the Baltic Sea and inland lakes of northern Europe. The simulated changes in these water bodies are discussed with emphasis on the wintertime ice conditions. Comparison with an earlier RCA experiment indicates that a physically consistent treatment of these water bodies is also of importance for the simulated atmospheric climate change.

1. Introduction

Predicting climate changes and future climate on the regional scale is a very challenging but an important task since, in practice, the impacts of climate change need to be studied on the regional rather than global scale. One of the several techniques being used for this task is regional climate modelling, also known as dynamical downscaling (Giorgi and Mearns, 1991, 1999; McGregor, 1997). In this approach, a high-resolution limited-area model (regional climate model = RCM) is run with boundary data taken from a global general circulation model (GCM) simulation. The technique is motivated partly by the fact that high-resolution regional models should better than GCMs account for mesoscale forcings such as complex topography and regional water bodies that modify the regional climate. In addition, increased resolution may add detail to the simulated weather systems, thereby leading to a more realistic simulation of daily weather variability (Christensen et al., 1998).

Regional climate simulations for an area covering northern and central Europe have been recently conducted at the Rossby Centre, which is part of the SWEdish regional CLImate Modelling programme SWECLIM. These experiments use boundary data from two atmosphere–ocean

* Corresponding author.
e-mail: Jouni.Raisanen@smhi.se

GCMs, HadCM2 (Johns et al., 1997; Mitchell and Johns, 1997) and ECHAM4/OPYC3 (Roeckner et al., 1996, 1999; Oberhuber, 1993). As the first step, the regional model was run at 88 km resolution. The control ('present-day') climates in these simulations were discussed by Rummukainen et al. (2000). Here we study the climate changes obtained by also running the regional model with boundary data from increased greenhouse gas simulations with the two GCMs.

In RCM climate change studies reported to date (Giorgi et al., 1994; Jones et al., 1997; Renwick et al., 1998), only one driving GCM has been used. However, the control climate in regional models is strongly affected by the boundary conditions (Noguer et al., 1998), and this is also necessarily the case with the simulated climate changes. Using two driving GCMs allows a quantitative approach on this issue. It is of particular interest to ask how much a RCM actually modifies the climate change in a driving GCM. If this modification would be large compared with typical differences between different GCMs, and attributable to factors better presented in a high-resolution RCM than a GCM (rather than to different parameterizations or dynamical problems associated with the nesting technique), this would suggest a drawback in the direct use of GCM results in constructing climate change scenarios. Conversely, if this relative modification turns out to be small, then GCM and RCM results are likely to be equally useful in terms of scenario construction. The answer to this question depends, most likely, on the aspect of climate change studied (and probably also on the area considered). The present analysis only focuses on changes in time mean surface air temperature and precipitation.

An important issue in the interpretation of climate change experiments is the impact of internal variability. As the experiments discussed here are short (10 years for both the control and scenario runs), the results are expected to contain a substantial amount of noise. It is therefore essential to try to estimate the signal-to-noise ratio in the obtained fields of climate change. This is particularly important regarding the differences in climate change between the two regional experiments with different driving GCM simulations. Would it turn out that these differences are not much larger than what is expected from internal variability, then they could likely be reduced substantially just by using longer time slices from the same GCM experiments to drive the RCM. Conversely, if the relative impact of internal variability would appear small, then the lengthening of the simulations would probably not help much. It is likewise important to estimate the importance of internal variability for the differences in climate change between the RCM and the driving GCM.

Another topic discussed here are the changes in the Baltic Sea and inland lakes (mainly the ice conditions) that may accompany a greenhouse-gas induced warming in northern Europe. The Rossby Centre regional model with its explicit model components for both the lakes and the Baltic Sea provides a suitable platform for addressing this issue, unlike the two GCMs that exclude lakes and resolve the Baltic Sea only very crudely. The extent to which these water bodies modify the simulated change in atmospheric climate is not easily determined, but some results from an earlier version of the same regional model are shown to illustrate that a bad representation of them may actually have adverse consequences.

The paper starts by describing briefly the Rossby Centre regional climate model (Section 2) and the driving GCM experiments (Section 3). Section 4 compares the changes in temperature and precipitation in the two GCMs and the two regional simulations, including several aspects of statistical analysis and some physical interpretation. The changes in the Baltic Sea and Nordic inland lakes are discussed in Section 5. The paper ends with a summary and some further discussion in Section 6.

2. The RCA1 regional climate model

The version RCA1 of the Rossby Centre regional Atmospheric climate model RCA is described in some detail by Rummukainen et al. (2000). It is based on the limited area weather forecast model HIRLAM (Källén, 1996; Eerola et al., 1997) used operationally in several European countries, but the land surface and snow scheme has been changed and separate modules have been added for inland lakes and the Baltic Sea. The model is run, in the present set-up, in a rotated latitude-longitude grid with a resolution of 88 km and with 19 hybrid levels between the surface and 10 hPa. It is forced by the driving GCM from its

lateral boundaries (8-point relaxation zones are used) and from below, by sea surface temperatures (SSTs) and deep soil temperatures.

The driving model SSTs are not used for the Baltic Sea, which is modelled following the approach of Omstedt and Nyberg (1996) as 13 vertically resolved sub-basins (see also Rummukainen et al. (2000)). The model simulates the average temperature and salinity profile within each sub-basin, taking into account vertical mixing, interaction with the atmosphere, and parameterized in- and outflows with neighbouring sub-basins. Lake temperatures are also modelled in an interactive manner in an area covering approximately the Baltic Sea drainage basin (Fig. 1; this restriction in area has partly historical reasons and can be relaxed with suitable physiographical data bases). The lake module (Ljungemyr et al., 1996; Omstedt, 1999) treats shallow (mean depth less than 10 m) lakes with a 0-dimensional energy balance model and deep lakes (mean depth over 10 m) with a vertically resolved model. Ice cover and thickness are also simulated in both the Baltic Sea and inland lake modules. In addition to ice thermodynamics, dynamic ridging processes are described for the deep lakes and the Baltic Sea.

One of the HIRLAM parameterizations this far retained in RCA is the radiation scheme of Savijärvi (1990) and Sass et al. (1994). A weakness of this scheme in climate change studies is that the impact of CO_2 is presented in a highly parameterized way, with a few constants tuned for present conditions. Deducing how these constants would change with increasing CO_2 is not straightforward and they were therefore not changed for the experiments reported here. Thus, the ultimate driving force of climate change in the two GCM experiments is lacking from RCA. This complicates the interpretation of the RCA results to some extent, although much of the effects of increased CO_2 are transmitted to RCA by the lateral and lower (SSTs and deep soil temperatures) boundary conditions obtained from the GCM simulations. A revision to this radiation scheme that allows for changing CO_2 and alleviates some other known weaknesses of the original HIRLAM scheme has

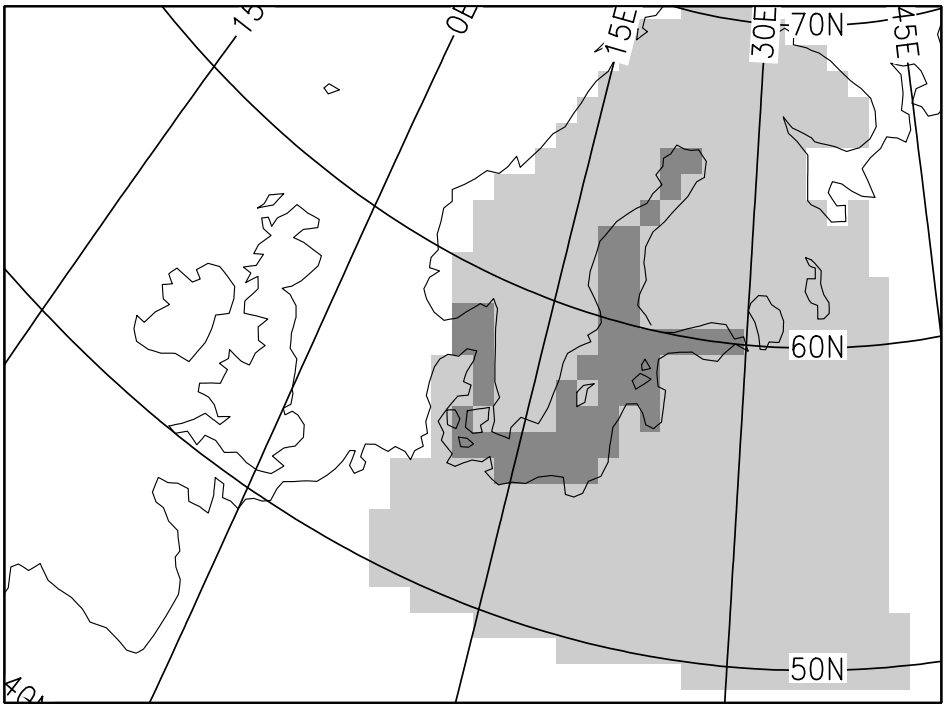

Fig. 1. The RCA model area excluding the 8-point boundary relaxation zones. The Baltic Sea is indicated by the dark shading and the area where the lake module is applied by the light shading.

been developed recently (Räisänen et al., 2000). The first one-year tests with the revised scheme give, among other things, an estimate of the bias that was caused to the RCA results by neglecting the increase in CO_2 (Subsection 4.4).

3. The GCM data sets

The RCA regional climate change experiments discussed in this paper got their boundary data from global climate simulations made with two atmosphere–ocean GCMs, HadCM2 (Johns et al., 1997; Mitchell and Johns, 1997) and ECHAM4/OPYC3 (Roeckner et al., 1996, 1999; Oberhuber, 1993). The latter of these is here briefly referred to as ECHAM4. For both models, two slightly over 10-year time slices were used, one acting as a control period and the other as a scenario period representing a future with higher greenhouse gas concentrations. No sulphate aerosol forcing is included in these GCM experiments.

The boundary data for the first regional experiment, denoted as RCA-H, are from partial reruns* of two long HadCM2 simulations: a control run and a transient greenhouse run, in which gradually increasing CO_2 represents the change in greenhouse gas forcing from the pre-industrial era. In the HadCM2 model years, the used period extends from 2039 to 2049. The other experiment, RCA-E, got its boundary data from a present-day (nominally 1980s) and a future (2070s) time slice from a transient ECHAM4 greenhouse run (as with RCA-H, the first of these was a rerun). The choice of periods in RCA-E involves, in principle, a risk that the GCM simulated climate change would be contaminated by climate drift that is unrelated to increasing greenhouse gases. This risk appears small since the parallel ECHAM4 control run is very stable between the periods considered, both regarding global mean temperature and precipitation and the climate in northern Europe. The increase in CO_2 between the two RCA-H time slices in HadCM2 is about 150% and the increase in equivalent CO_2 between the two RCA-E time slices in ECHAM4 (that treats explicitly CO_2, CH_4, N_2O and several CFCs) slightly over 100%. The difference between the two experiments in global mean radiative forcing is smaller, from Fig. 0.3 of Machenhauer et al. (1998) about 20% (5.4 $W\,m^{-2}$ in HadCM2 versus 4.5 $W\,m^{-2}$ in ECHAM4), since radiative forcing is a logarithmic rather than a linear function of CO_2 and the amplitude of this proportionality is slightly model-dependent.

Thus, the boundary data time slices for RCA-H and RCA-E search to represent somewhat different periods. In spite of this, the increase in global mean temperature between the two time slices is almost the same, 2.6°C, in both HadCM2 and ECHAM4. The two RCA experiments give, therefore, two quantitatively comparable scenarios of how climate in northern Europe might change along with a greenhouse gas induced 2.6°C global mean warming. The uncertainty in the timing of this warming is, however, not reflected in the comparison.

The climates in the RCA control runs and their relation to the control climates in the driving GCMs were discussed by Rummukainen et al. (2000). The GCM simulations were generally found to be of reasonably high quality (compared with the errors typically present in current atmosphere–ocean GCMs), but some marked biases were also identified. HadCM2 was found to have a general cold bias in surface air temperatures in spring and summer, which reaches 3–4°C in the Nordic Countries in July. ECHAM4 showed typically smaller but mostly positive temperature biases. Precipitation biases were found to be geographically variable, but considering the RCA domain as a whole, the precipitation in both GCMs is above the CRU climatology (Hulme et al., 1995) in winter and spring (although this is partly attributable to an undercatch of the actual precipitation in measurements) and somewhat below it in summer. The biases in RCA-H and RCA-E followed more or less closely the driving GCM results. RCA showed generally higher skill than the GCMs in simulating the geographical distribution of temperature and precipitation within the model area, but it had no systematical tendency to either reduce or worsen the large-scale biases in the driving GCM simulations. In RCA-E, a mismatch between the functioning of

* Reruns were needed to obtain a data set detailed enough for driving RCMs. Because of the use of a different computer and a chaotic amplification of the associated (initially) bit-level differences, these reruns are not identical with the same decades in the original longer HadCM2 simulations.

the RCA and ECHAM4 moist physics resulted in very little precipitation in the boundary relaxation zones, with sharp gradients in precipitation near the inner edges of these. To keep this problem further away from the areas of interest, the model domain in RCA-E was widened slightly (by four grid boxes in the north and two grid boxes in the other directions) from that used in RCA-H.

The present analysis of climate changes in the RCA-H and RCA-E experiments uses full 10 years of data for both two control and scenario time slices. The first 3–6 simulated months preceding this 10-year period are neglected to avoid spinup. Some residual spinup might still occur in the slowest model components (deep soil, Baltic Sea and lakes) during the beginning of the analysed period, but the impact of this was judged negligible compared with the strong interannual variability.

For comparison with RCA, the results of the driving GCMs were interpolated bilinearly to the denser RCA grid. In Section 4, some statistical analysis is made separately for the large-scale and sub-GCM scale parts of the RCA fields. The large-scale part is obtained by first aggregating the RCA results to the grid boxes of the driving GCM (2.5° lat × 3.75° lon in HadCM2 and 2.8° × 2.8° in ECHAM4), and by then interpolating bilinearly back to the RCA grid. The sub-GCM scale part is the difference between the total and the large-scale part. This differs slightly from the large-scale–mesoscale division of Giorgi et al. (1993, 1994) and Jones et al. (1995, 1997), who defined the large-scale part, for each RCM grid box, as an average over a specified number of surrounding grid boxes. The present approach has the advantage that the sub-GCM part of the GCM solution is zero (this does not formally hold for the Giorgi et al. mesoscale part when this is calculated from GCM results interpolated to the RCA grid). In practice, however, the difference is small. The Giorgi et al. method with an averaging area of 5 × 5 grid boxes (440 km × 440 km; similar to Jones et al. (1995, 1997)) turned out to yield very similar statistics of small-scale climate change as the present approach.

In Section 4, various statistics are used. These are calculated over those RCA grid boxes that have a fraction of land of at least 50%, excluding the 8-point relaxation zones in RCA-H and the extension of the RCA-E grid over RCA-H. The focus is on land partly because land areas are of largest interest from a human perspective, partly because the temperature response over the Atlantic Ocean is essentially determined by the SSTs taken from the GCM simulations.

4. Changes in surface climate: comparison between RCA and the driving GCMs

4.1. General

The simulated changes in winter (December–February = DJF), summer (June–August = JJA) and annual mean temperature in the two RCA experiments are shown at the first and third rows of Fig. 2. The annual mean warming is, in most of the land area, around 3°C in RCA-H and 3–4°C in RCA-E. The seasonal cycle of the simulated warming in northern Europe is also similar in the two experiments, with larger warming in winter than in summer. In the southern half of the model area, however, RCA-E indicates a much stronger warming in summer than in winter, which is generally not the case in RCA-H. Substantial differences occur over the northern North Atlantic, where RCA-H shows a much more distinct minimum in warming than RCA-E, and in the finer geographical details of the change over land. For example, the wintertime warming in eastern Finland and northern Russia is several degrees larger in RCA-E than in RCA-H.

The simulated warming in each of the two RCA experiments resembles closely the warming in the driving GCM (the second and fourth rows of Fig. 2). This is trivial over the Atlantic Ocean where the SSTs in RCA are taken directly from the driving model, but it is generally true even over the land areas. Some differences do occur; in particular, the warming in RCA-H is typically slightly smaller than that in HadCM2 and the warming in RCA-E slightly smaller than that in ECHAM4.

Similar maps for precipitation change are shown in Fig. 3. The two RCA experiments agree on a general increase in annual precipitation in northern Europe, but the differences in the seasonal and geographical distribution of the change are substantial. In particular, the RCA-H experiment yields a very large increase (up to over 80% of the control run mean) in summer precipitation around the Baltic Sea, where RCA-E indicates little change. In central Europe, RCA-E shows a

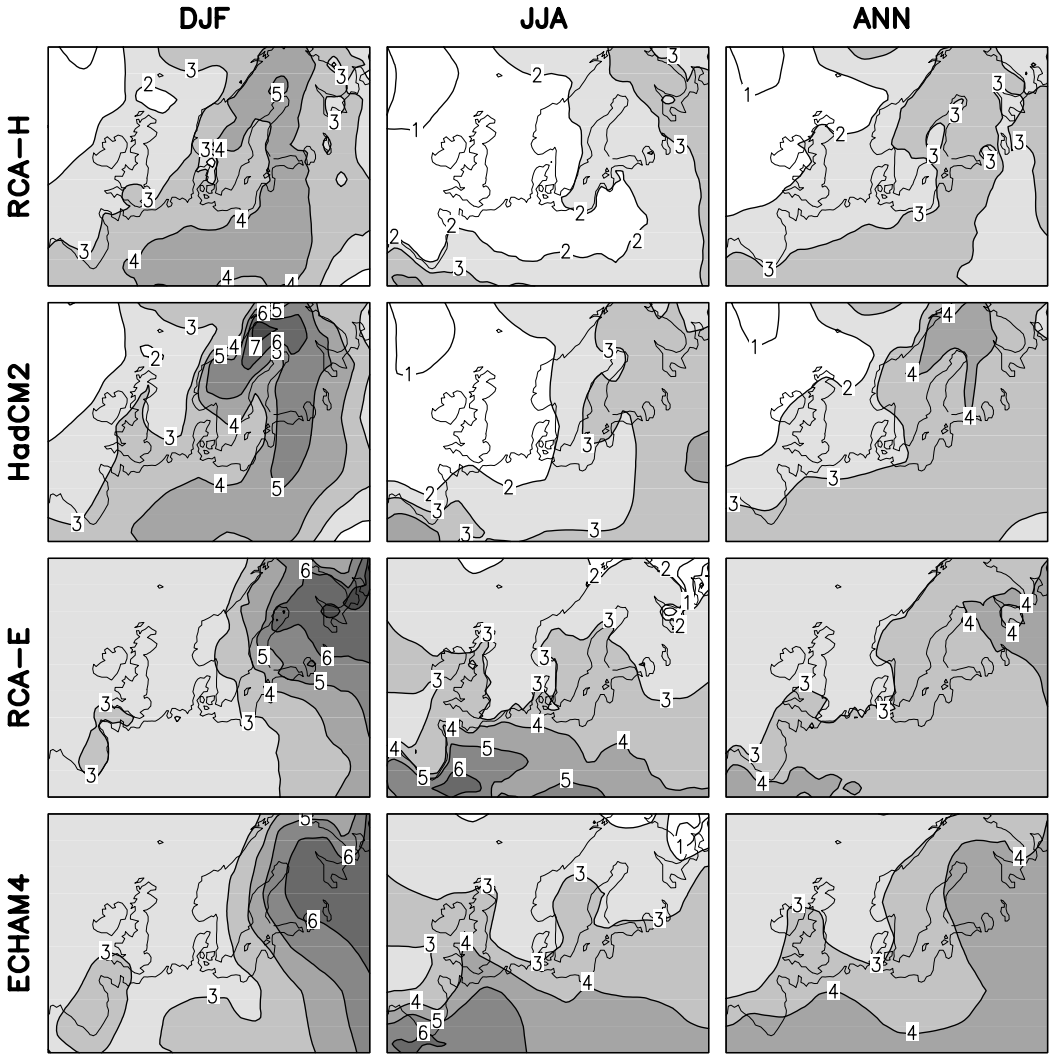

Fig. 2. 10-year mean changes (scenario–control) in surface air temperature (°C) in December–February (left), June–August (middle) and the annual mean (right). From top to bottom: RCA-H, HadCM2, RCA-E and ECHAM4. Areas with a warming of over 2°C are shaded with progressively darker shading for increasing warming.

slight decrease in annual precipitation which mainly results from larger decreases in summer and autumn, whereas slight increases dominate in RCA-H in most of this area. The seasonal variation of the simulated precipitation changes is irregular and only crudely captured by the winter and summer means shown in Fig. 3. For example, the largest increase in precipitation in northern Europe in RCA-E actually occurs in autumn.

As expected from the higher resolution, the RCA experiments show a much more detailed geographical structure in precipitation change than the driving GCMs. On larger scales, however, RCA-H is reasonably similar to HadCM2 and RCA-E reasonably similar to ECHAM4, at least in comparison with the differences between the two GCM (or two RCA) simulations themselves.

The differences RCA-H–HadCM2 and RCA-E–ECHAM4 in annual temperature and precipitation change are shown in Fig. 4. As already noted,

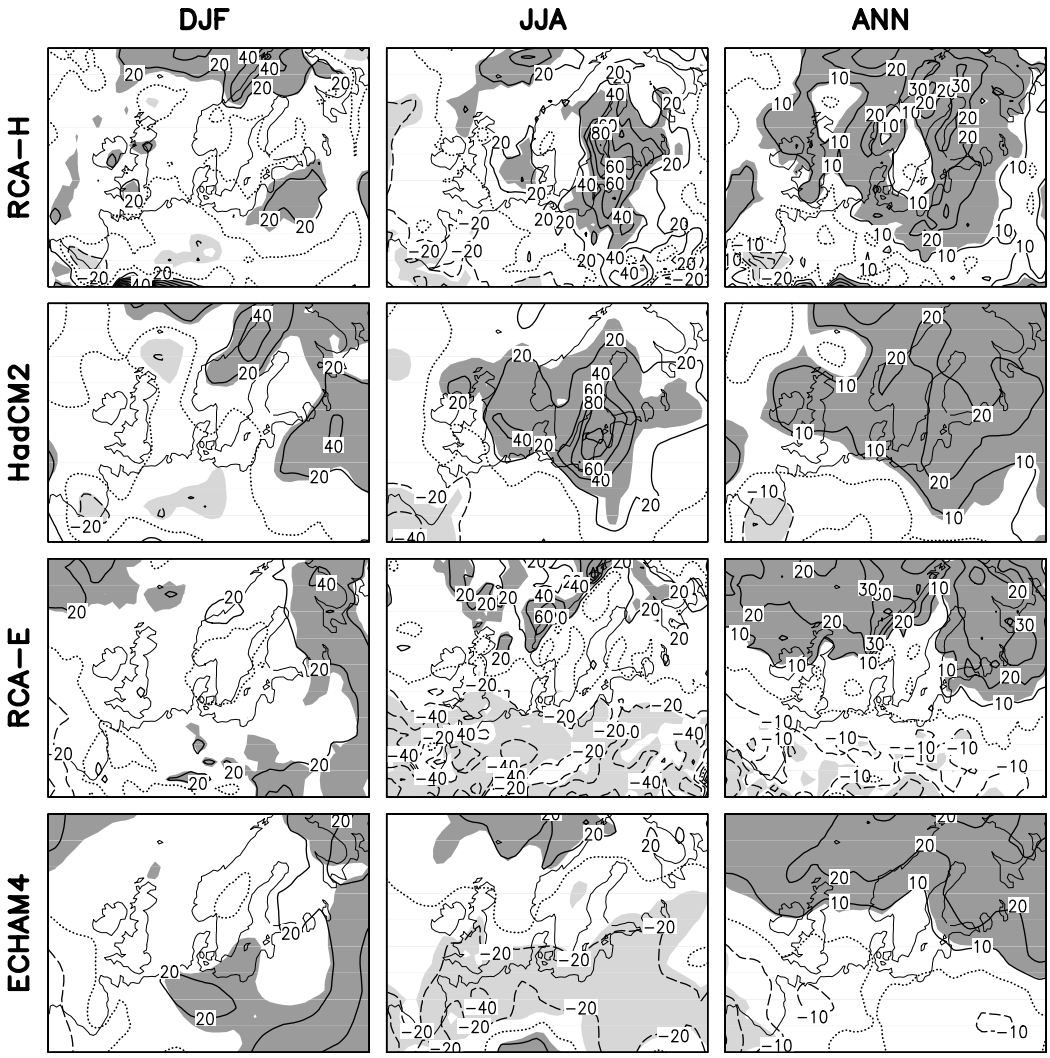

Fig. 3. Relative changes in precipitation (% of control run mean) in December-February (left), June–August (middle) and the annual mean (right) in the two RCA experiments and in the driving GCMs. Contour interval is 20% for seasonal and 10% for annual mean changes. Increases (decreases) significant at the 90% level are shaded in dark (light).

RCA-H and RCA-E both have an overall tendency to moderate the temperature increase simulated by the driving GCM. The geographical details (and seasonal cycle, not shown) of this modification differ between the two pairs of experiments, but in both cases, a relatively large annual mean difference (over 0.5°C) occurs in the eastern part of the model domain. The differences in precipitation change show a more noisy pattern, but some larger-scale structures are also evident (for example, in central Europe RCA-H indicates generally more positive changes than HadCM2 but RCA-E more negative changes than ECHAM4). As also indicated in Fig. 4, the RCA–GCM differences in temperature change are generally better discernible from internal variability than the differences in precipitation change. The importance of internal variability for the interpretation

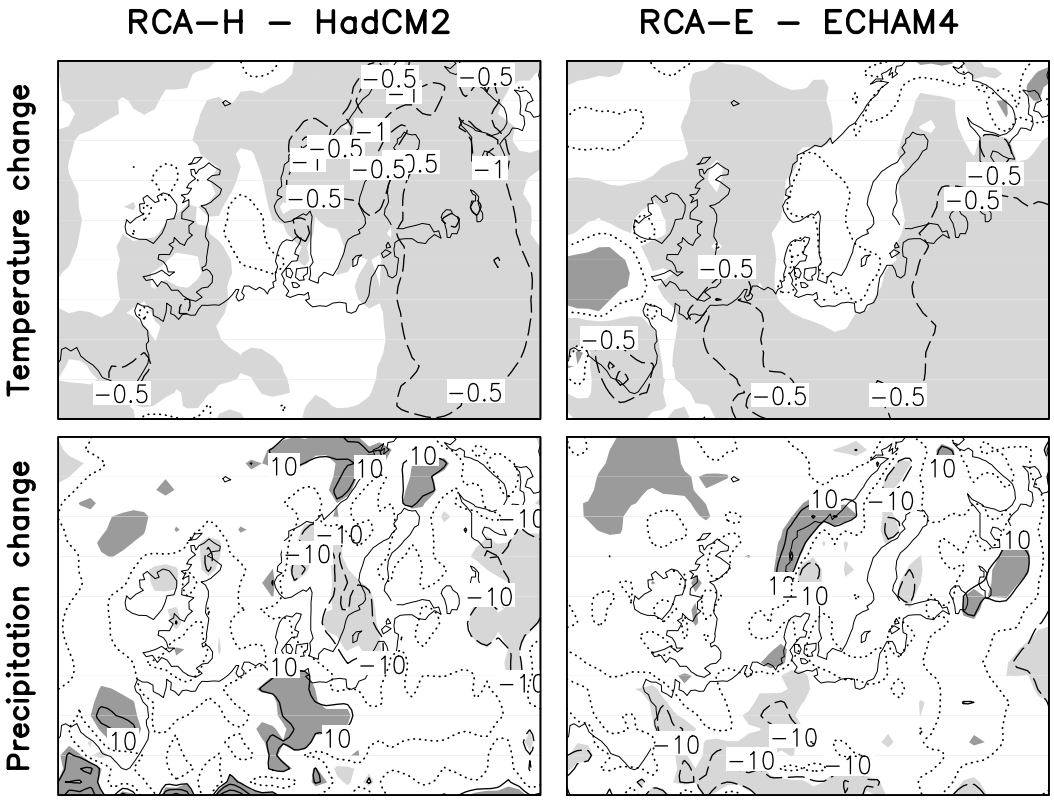

Fig. 4. Differences in annual mean temperature (contour interval 0.5°C) and precipitation change (contour interval 10%) between RCA and the driving model (RCA-H–HadCM2 and RCA-E–ECHAM4). Areas where the change is at the 90% significance level more positive (more negative) in RCA than in the driving model are shaded in dark (light).

of the RCA experiments will be addressed more thoroughly in Subsection 4.3.

4.2. *Root-mean-square differences and relative similarity*

A more quantitative view on the differences between the various experiments is provided in Fig. 5. Seasonal and annual land area root-mean-square (rms) differences in temperature and precipitation change are shown for four model pairs: ECHAM4–HadCM2 (below: ECH–Had), RCA-E–RCA-H (RCA–RCA), RCA-H–HadCM2 (RCA-H–Had) and RCA-E–ECHAM4 (RCA-E–ECH). As noted in Section 3, the GCM results were interpolated bilinearly to the RCA grid and the RCA–GCM differences on that grid include contributions from both the GCM-resolved scales and from details unresolvable by the GCMs. The rms amplitudes are shown in Fig. 5 for both of these. For RCA–RCA, the large-scale (sub-GCM scale excluded) as well as the total rms differences are given. Note that the sub-GCM scale and large-scale differences are not additive in terms of the rms amplitude. In fact, the large-scale RCA–GCM rms differences in temperature change are occasionally slightly larger than the total rms differences. In those cases, the large-scale rms difference is not shown separately.

Several points of interest may be noted from the figure:

(1) In terms of temperature change, the two RCA experiments are approximately as far from each other as the driving GCM experiments. By contrast, the RCA–RCA rms difference for

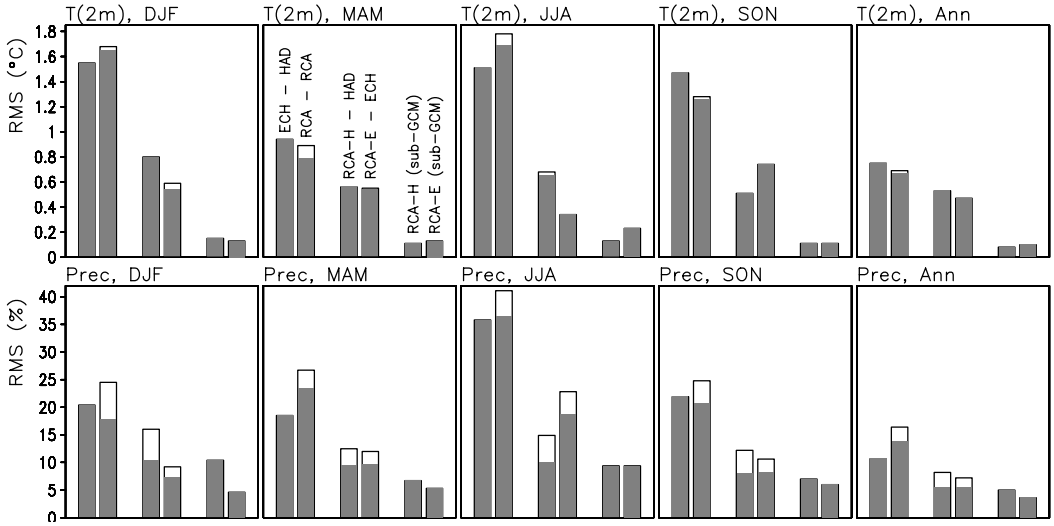

Fig. 5. Land area rms differences in seasonal and annual mean temperature (°C) and precipitation (%) change between different experiments. In each panel, the first and the second bar show the differences ECHAM4–HadCM2 and RCA-E–RCA-H, and the next two the differences between RCA and the driving GCM (RCA-H–HadCM2 and RCA-E–ECHAM4). For the RCA–RCA and RCA–GCM differences, the full bar length shows the total difference and the filled part the large-scale difference obtained by removing from the RCA results the sub-GCM scale details. For the RCA–GCM differences in temperature change, the large-scale rms amplitude is occasionally slightly larger than the total rms amplitude and is then not shown separately (see text). The rms amplitude of the sub-GCM scale details of climate change in RCA-H and RCA-E is shown by the last two bars.

precipitation changes is in all seasons and in the annual mean larger than the ECH–Had difference. This is due to the higher resolution of RCA, which enables it to resolve smaller-scale details of precipitation change than the GCMs. The large-scale rms differences between the two RCA experiments are similar to the ECH–Had differences even in the case of precipitation change.

(2) As suggested by Figs. 2 and 3, the rms differences between RCA and the driving GCM are smaller than the rms differences between the two GCMs or the two RCA simulations themselves. All in all, the RCA–GCM rms differences vary between 23% (temperature, RCA-E–ECH, JJA) and 79% (precipitation, RCA-H–Had, DJF) of the corresponding ECH–Had rms differences.

(3) The RCA–GCM differences in temperature change are dominated by the GCM-resolved scale. Sub-GCM scale temperature changes in RCA are generally quite weak. Sub-GCM scale details of precipitation change are of a somewhat more appreciable magnitude, in agreement with Jones et al. (1997), but they still have in most cases a smaller rms amplitude than the large-scale RCA–GCM differences.

If generalizable, the first two points above also suggest that regional climate modelling will not lead to reduced spread in projections of future temperature and precipitation change. The spread appears to be, even on the grid box scale, governed by the driving GCM results, and to the extent that a RCM actually modifies the results of different GCMs, these modifications do not necessarily lead to reduced differences in climate change between the regional simulations. The third point complicates the interpretation of the RCA–GCM differences. While sub-GCM scale details of climate change in a RCM simulation are (reliable or unreliable) new information, the RCA–GCM differences on larger scales might reflect weaknesses in either RCA or the driving GCM, or both.

To complement the discussion of differences, it is useful to compare the two RCA experiments even in terms of their relative similarity. In Table 1,

a nondimensional statistics

$$s = \frac{\overline{AB}}{\overline{(A^2 + B^2)}/2} \quad (1)$$

(to be referred to as similarity) is used for this. A and B denote the climate changes in RCA-H and RCA-E, and the overline indicates a land area mean. s is identical with the uncentred correlation apart from a difference in the denominator that makes it sensitive to differences between the area means of A^2 and B^2. s only attains its maximum value of 1 when $A = B$ in the whole area of comparison. Conversely, the value $s = -1$ indicates that A and B are exactly the opposite.

This statistics indicates a high similarity (from 0.85 in JJA to 0.98 in the annual mean) between the temperature changes in RCA-H and RCA-E, emphasising that the differences between the two experiments are relatively small compared with the overall magnitude of the simulated warming. There is also a reasonable (0.63 or above) similarity between the *differences* RCA-H–Had and RCA-E–ECH in the simulated temperature change in MAM, SON and the annual mean. This mainly reflects the general weakening of warming in RCA relative to the driving GCM, which occurs in both of RCA-H and RCA-E but is unlikely to be an improvement (Subsection 4.4). Some similarity between the two RCA experiments occurs, however, even in the sub-GCM scale details of temperature change (up to $s = 0.56$ in the annual mean). This is mainly related to more sharply resolved coastlines in RCA than in the driving models.

The precipitation changes in RCA-H and RCA-E are much less similar than the temperature changes, s varying from only 0.03 in JJA to 0.49 in SON. Furthermore, taking the fields as a whole, the differences between RCA and the driving model are essentially unrelated between the two experiments. On the sub-GCM scale, there is some modest similarity between RCA-H and RCA-E in the annual mean and in SON, but hardly in the other seasons.

One very probable contributor to the weaker similarity of precipitation than temperature changes between RCA-H and RCA-E is the fact that the precipitation changes are much less well discernible from internal variability in the simulations. Internal variability is of importance even in interpreting many other aspects of the results discussed this far. This issue is therefore studied in some detail in the next subsection. Some physical issues related to the interpretation of the RCA–GCM differences in climate change are discussed in Subsections 4.4–4.5.

4.3. Rôle of internal variability

The climate changes in the RCA experiments are calculated as seasonal or annual 10-year mean differences between a scenario run and a control run. Because of internal (i.e., unforced) variability in the modelled (GCM + RCA) climate system, non-negligible differences between two such 10-year averages might occur just by chance. It is important to estimate how well the simulated climate changes and differences in climate change between different experiments are discernible from this inherent noise.

Estimates of the statistical significance of the results were already included in Figs. 3 and 4. The significance of climate changes in each of the two RCA experiments was inferred from the t-statistics

$$t = \frac{S - C}{\sqrt{(V_C + V_S)/(n-1)}}, \quad (2)$$

where S and C are the n-year (here $n = 10$) seasonal or annual means of variable X in the

Table 1. *Similarity (1) between RCA-H and RCA-E in temperature and precipitation change, in the difference of temperature and precipitation change from the driving GCM, and in the sub-GCM scale temperature and precipitation change*

	Temperature change					Precipitation change				
	DJF	MAM	JJA	SON	Ann	DJF	MAM	JJA	SON	Ann
total change	0.91	0.95	0.85	0.94	0.98	0.19	0.11	0.03	0.49	0.40
difference from GCM	0.09	0.63	0.28	0.81	0.74	0.00	0.13	−0.12	0.07	−0.07
sub-GCM scale	0.20	0.18	0.43	0.45	0.56	−0.07	0.15	0.03	0.28	0.35

scenario run and the control run and V_S and V_C the interannual variances within these runs. This form assumes that individual years are independent from each other. The 240-year HadCM2 and ECHAM4 control runs available via the IPCC Data Distribution Centre suggest that this is a good assumption for precipitation, but not fully justified for temperature. For example, the actual interdecadal variance of annual mean temperature is, as averaged over these two simulations and the RCA land area, about 25% higher than estimated from interannual variability within individual decades. The test (2) is therefore likely to be slightly non-conservative for temperature changes. Likewise, the quantitative estimates of the relative importance of unforced temperature variability presented below are probably somewhat too small. We choose to accept this bias, rather than using the interdecadal variability in the GCM control runs, because the latter alternative involves other potential sources of error due to differences in the magnitude of variability between RCA and the GCMs and between the control and the scenario runs.

To address the significance of the difference in temperature change between RCA (subscript 1) and the driving GCM (subscript 2), the test (2) was applied to the means and variances of the temperature difference between these models:

$$\Delta X = X_1 - X_2. \tag{3}$$

Thus, the difference in climate change is judged to be statistically significant if the mean difference between RCA and the driving model in the scenario run differs significantly from the same difference in the control run. For precipitation change, measured here in per cent, (3) was replaced with

$$\Delta X = X_1 - AX_2 \tag{4}$$

where the scaling factor

$$A = \frac{C_1 + S_1}{C_2 + S_2} \tag{5}$$

ensures that $t = 0$ when the relative changes in RCA and the driving model are the same.

Using these tests, the changes in seasonal and annual mean temperature in the two RCA experiments (or the two GCMs) are significant at the 90% level ($|t| > 1.734$) in virtually the whole model domain. The differences in annual mean temperature change between RCA and the driving GCM (RCA-H–HadCM2; RCA-E–ECHAM4) are also at this level significant in over 70% of the land area, but the same fraction for seasonal differences is in some cases substantially lower (Table 2). Precipitation changes in RCA-H and RCA-E are significant in less than a half of the area in the annual mean, and significant seasonal changes are in most cases even less frequent. The fraction of statistically significant differences in seasonal and annual precipitation change between RCA and the driving model never exceeds 24%, and in one case (RCA-H–HadCM2 in JJA) it falls below the 10% on the average expected from pure chance.

A more quantitative approach to the same issue is to estimate the magnitude of error in the simulated climate change (or inter-experiment differences in climate change) that would on the average be expected to arise from internal variability. In the following, such error estimates are derived for the RCA experiments. To get an idea of the signal-to-noise ratio, these estimates are then compared with the actual magnitude of the simulated climate changes or differences in these.

The expected magnitude of error is characterized, in principle, by the variance that would be obtained by repeating the climate change experiment a large number of times with different initial conditions (in case of regional simulations, this would require varying the initial conditions in the driving GCM as well). Having no such ensembles available, this variance is estimated from the interannual variability in the simulations, neglecting interannual autocorrelation (which in the case of temperature changes is likely to make the estimates slightly too small). For temperature changes in RCA-H and RCA-E, this estimated error variance is just the denominator of (2)

$$V = \frac{V_C + V_S}{n - 1}. \tag{6}$$

For the difference in change between RCA-H and RCA-E, the outcome of (6) is summed up over these two experiments. For RCA-H–HadCM2 and RCA-E–ECHAM4, V_C and V_S are calculated as the control and scenario run variances of the difference from the driving model, as in (3), to take into account the fact that the interannual variations in RCA and the driving model are correlated.

The same calculation for relative precipitation

Table 2. *Fraction (%) of statistically significant (90% level) temperature and precipitation changes in RCA-H and RCA-E, and that of statistically significant differences in temperature and precipitation change between RCA and the driving GCM*

	Temperature change					Precipitation change				
	DJF	MAM	JJA	SON	Ann	DJF	MAM	JJA	SON	Ann
RCA-H	99	100	100	100	100	23	34	21	24	46
RCA-E	100	100	100	100	100	31	27	45	47	41
RCA-H–HadCM2	33	49	42	37	72	24	12	7	14	24
RCA-E–ECHAM4	52	64	21	76	74	16	20	23	19	24

change is more complicated because the sensitivity of the relative change to variations in the control run mean increases with the relative change itself (Section 8). Based on perturbation analysis, the error variance for each of RCA-H and RCA-E is estimated as

$$V = \frac{V_S + (S^2/C^2)V_C}{(n-1)C^2}. \tag{7}$$

For the difference in precipitation change between RCA and the driving model, similar analysis leads to the approximate result

$$V = \frac{1}{n-1}\left[\mathrm{VAR}\left(\frac{S_1}{C_1^2}X_{1,C} - \frac{S_2}{C_2^2}X_{2,C}\right) + \mathrm{VAR}\left(\frac{1}{C_1}X_{1,S} - \frac{1}{C_2}X_{2,S}\right)\right], \tag{8}$$

where VAR( ) indicates the interannual variance of the expression in the parentheses, and $X_{1,C}$ ($X_{2,S}$) are the yearly precipitation values in the RCA control (GCM scenario run). At levels of interannual precipitation variability typical in the RCA model area and for zero interannual autocorrelation, (7) and (8) may have a small (of the order of a few per cent) positive bias (Section 8).

As an example, the results of this calculation for winter (DJF) mean temperature change in RCA-H and for the differences RCA-H–HadCM2 and RCA-H–RCA-E are shown in Fig. 6 (using the standard error defined as the square root of the estimated variance). The standard error in RCA-H increases eastward but is typically of the order of 1°C. For the difference RCA-H–HadCM2, however, the same figure is below 0.5°C in most of the area. Because interannual temperature variations in RCA and its driving GCM are correlated, the difference in temperature change between them is less uncertain in absolute terms than the temperature change in either of them individually. Conversely, the standard error for the difference between the RCA-H and RCA-E experiments (which are independent in terms of internal variability) is always larger than that for either of these two. Regarding temperature change, winter is the worst case since this is the season when interannual temperature variability is largest. The standard errors for the annual mean change are only

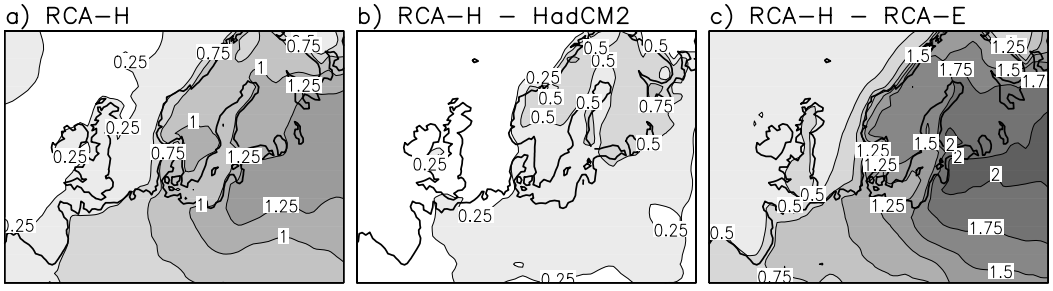

Fig. 6. Standard error due to internal variability (see text) in December–February temperature change: (a) RCA-H, (b) difference RCA-H–HadCM2, (c) difference RCA-H–RCA-E. Contours at every 0.25°C.

about 40% of the winter values. On the other hand, in comparison with the general magnitude of the simulated changes, the standard errors for precipitation change are larger than those for temperature change.

In any individual grid box, the climate changes in RCA-H and RCA-E might be either much further from or much closer to their real noise-free values than suggested by (6) and (7), and the same applies to the differences between the different experiments. However, when the variances are averaged over a larger area, the estimates gradually become more meaningful. In Table 3, the relative importance of internal variability to the simulated climate changes (or differences in these between different experiments) in the whole RCA land area excluding the boundary zones is estimated. These estimates are obtained by dividing the area mean variances from (6)–(8) by the corresponding mean squares of the simulated climate change (or differences in change between different experiments). A ratio of about 0.5 suggests that the climate change signal and the noise are of comparable magnitude, whereas a smaller (larger) ratio indicates that the signal (the noise) dominates. It is seen that

(1) Temperature changes in both of RCA-H and RCA-E are much larger than the error expected from internal variability, but this is not true for precipitation changes. In each four seasons, more than a half of the simulated precipitation changes is attributed to internal variability in at least one of RCA-H and RCA-E. In the annual mean, however, the signal appears to dominate over the noise in both of these.

(2) Only about 10% of the differences in annual mean temperature change between RCA and the driving GCMs seem to arise from internal variability. Even in the individual seasons, the same ratio is with one exception 31% or lower. By contrast, internal variability apparently accounts for about a half of the RCA–GCM differences in annual precipitation change, and typically for an even larger fraction of the seasonal differences. In one case (RCA-H–HadCM2 in JJA), the actual differences in precipitation change are slightly smaller than on the average expected from internal variability alone. This must be taken as a result of sampling problems or other sources of error in the calculation, rather than as an indication of that the differences would disappear completely if internal variability could be eliminated.

(3) Although sub-GCM scale temperature changes in RCA are small, they are in general reasonably well discernible from internal variability (the noise on this scale is also weak because temperature variations in nearby grid boxes are highly correlated). However, excluding RCA-H in DJF and in the annual mean, a majority of the sub-GCM scale details in precipitation change seem to be noise.

(4) Typically about a half (or somewhat more) of the seasonal and annual RCA-H–RCA-E differences in climate change are attributed to internal variability. This is true for both temperature and precipitation, with somewhat larger

Table 3. *Estimated relative contribution of internal variability to temperature and precipitation changes in RCA-H and RCA-E, and to the differences RCA-H–HadCM2, RCA-E–ECHAM4 and RCA-E–RCA-H; the same ratio is also given for the sub-GCM scale contribution to the RCA-H and RCA-E changes (in parentheses)*

	Temperature change					Precipitation change				
	DJF	MAM	JJA	SON	Ann	DJF	MAM	JJA	SON	Ann
RCA-H	0.07	0.04	0.07	0.03	0.02	0.49	0.50	0.71	0.55	0.29
(sub-GCM scale)	(0.38)	(0.33)	(0.30)	(0.29)	(0.24)	(0.20)	(0.68)	(0.94)	(0.66)	(0.31)
RCA-E	0.08	0.05	0.02	0.01	0.01	0.63	0.60	0.29	0.23	0.25
(sub-GCM scale)	(0.54)	(0.25)	(0.13)	(0.27)	(0.16)	(0.79)	(0.82)	(0.69)	(0.64)	(0.51)
RCA-H–HadCM2	0.22	0.19	0.31	0.31	0.10	0.32	0.81	1.26	0.82	0.46
RCA-E–ECHAM4	0.31	0.13	0.54	0.08	0.08	0.65	0.64	0.41	0.74	0.53
RCA-E–RCA-H	0.79	0.94	0.22	0.29	0.73	0.69	0.61	0.47	0.66	0.45

seasonal variations in the ratio in the case of temperature change. In comparing these results with the corresponding ratios for the RCA–GCM differences, it is important to recall that the absolute impact of internal variability to the latter differences is smaller.

Thus, internal variability appears very important in interpreting the simulated precipitation changes and differences in them, but less important in the case of temperature changes, excluding the RCA-H–RCA-E differences. The results in Table 3 suggest that, if the RCA-H and RCA-E experiments had been made using longer time slices from the HadCM2 and ECHAM4 experiments, some of the differences in the resulting downscaled climate change might have been substantially smaller (the same of course applies to the original GCM-simulated changes as well). Likewise, the differences in climate change between RCA and the driving GCMs would have been smaller, at least concerning precipitation. Nevertheless, the results also suggest that some substantial differences in climate change between the different experiments would have remained even in the absence of internal variability.

4.4. *Temperature change and radiation*

As mentioned in Section 2, the RCA radiation scheme disregards variations in atmospheric CO_2. To overcome this limitation and some other known weaknesses of the scheme, some revisions to it have been developed recently (Räisänen et al., 2000). To study the impact of these revisions, three 14-month runs were made. The first of these (NEW1C) used boundary data from the beginning of the ECHAM4 control time slice. In the second run (NEW2S), boundary data from the beginning of the ECHAM4 scenario time slice were used and CO_2 was doubled from 353 to 706 ppmv to be broadly consistent with the ECHAM4 forcing scenario. In the third run (NEW1S), made for separating the impact of doubled CO_2 from other changes made to the radiation scheme, the scenario run boundary data were used but CO_2 was retained at 353 ppmv. The last 12 months of these runs were compared with the same periods of the original RCA-E simulations discussed above (OLD1C, OLD1S).

Fig. 7a shows the 12-month mean temperature difference (NEW2S–OLD1S)–(NEW1C–OLD1C). The revision generally induces a more positive change in the scenario run than in the control run temperature, thus amplifying the temperature difference between the two runs. In the land area annual mean, the difference is 0.24°C, which is a substantial part of the actual difference in average 10-year mean warming between ECHAM4 and RCA-E (0.37°C). The largest difference occurs in the southeastern part of the RCA domain, which is also the area where the 10-year ECHAM4–RCA-E difference (Fig. 4) is largest. A majority, but not all, of the difference

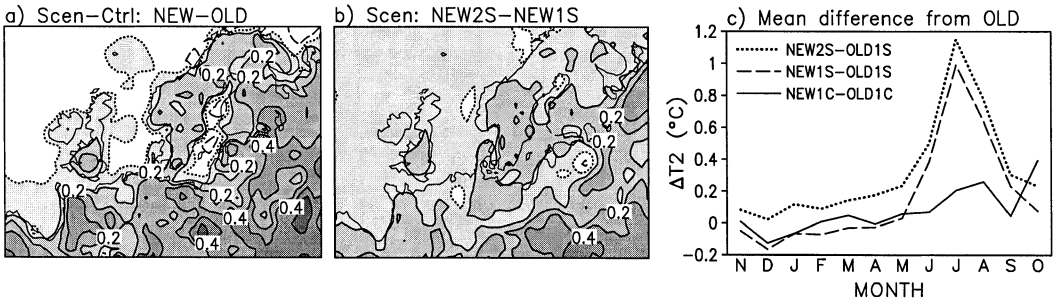

Fig. 7. Impact of the revised ("NEW") radiation scheme on surface air temperature in one-year runs. (a) The scenario–control change in the annual mean temperature difference between the new and the RCA1 ("OLD") scheme. (b) Contribution to (a) from doubling of atmospheric CO_2 in the new scheme. (c) Monthly land area mean temperature differences: new–old, control run (solid); new scheme with present CO_2–old scheme, scenario run (dashed); new scheme with doubled CO_2–old scheme, scenario run (dotted).

is associated with doubled CO_2 in NEW2S. The impact of this factor alone (NEW2S–NEW1S; Fig. 7b) is on the average 0.16°C. Had a similar test been made for the RCA-H time slices, this latter figure would probably have been somewhat larger because the increase in CO_2 in HadCM2 is 150% rather than 100%.

The land area mean temperature difference NEW2S–NEW1S resulting from doubled CO_2 is positive throughout the simulated period, with only moderate month-to-month variations. The other changes in the radiation scheme affect the simulated control and scenario climates in a more complicated way (Fig. 7c). The mean temperature in NEW1C is close to or slightly above that in OLD1C throughout the year. NEW1S is similarly close to OLD1S in most of the year, but substantially warmer in summer (almost 1°C in July). Thus, to the extent that this result would hold in longer simulations, the new scheme would amplify the simulated summertime warming even without changes in CO_2. This feature appears to be primarily associated with the calculation of long-wave (LW) radiation. The new scheme reduces considerably, in warm and humid summer conditions, the sensitivity of outgoing LW radiation to variations in surface temperature, which is probably associated with an improved treatment of the water vapour continuum absorption (Räisänen et al., 2000). Thus, the negative feedback between increasing temperature and increasing LW cooling is made weaker by the new radiation scheme.

4.5. *Changes in sea level pressure and precipitation*

Some of the RCA–GCM differences in precipitation change appear to result from interaction between the simulated changes in surface circulation and the different model orographies. For example, the change in annual mean sea level pressure in RCA-E indicates a strengthening of westerly winds across the Scandinavian mountains (Fig. 8). Associated with this is a sharp gradient in precipitation change, with larger increases on the western than on the eastern slope of the mountain range (Fig. 3). ECHAM4 simulates an almost identical change in the pressure pattern (not shown), but because of its lower resolution and smoother orography, the gradient in precipitation change is much more muted. A qualitatively similar but weaker gradient in precipitation change occurs in RCA-H, consistent with a similar but more vague change in the pressure pattern. HadCM2 shows a hint of a maximum in precipitation change right over the mountain range, but hardly any difference between the western and eastern slopes.

Thus, in areas of sharp orography, RCA appears able to produce a precipitation response that is physically more consistent with circulation changes than that in the driving GCMs. On the other hand, although the changes in sea level pressure in RCA-H and RCA-E are quite similar in the annual mean (over the land area, $s = 0.86$), there are much larger differences between them in some of the individual seasons (in DJF $s = 0.18$ and in JJA $s = 0.04$). This is not unexpected, since the simulated pressure changes have a relatively low signal-to-noise ratio. The diagnostics used in Subsection 4.3 suggest that the RCA-H–RCA-E differences in pressure change are, even when apparently sizeable, generally very hard to distinguish from the strong internal variability.

5. Baltic Sea and lakes

As noted in Section 2, RCA1 includes modules for the Baltic Sea and inland lakes of northern Europe. In this section, the simulated changes in these water bodies are discussed with emphasis on the wintertime ice cover. The average length of the ice season in northern Europe in the two RCA control and scenario runs and the control–scenario differences are shown in Fig. 9.

In the control runs, a slight tendency towards a too short lake ice season (on the average by about 20 days) was found (Rummukainen et al., 2000), at least regarding Swedish lakes for which verification data were available. Still, the lakes in northernmost Scandinavia were simulated to be ice-covered more than a half of the year, and an average ice season of several months occurred even in the other parts of the Nordic area, excluding Denmark and southernmost Sweden. In the scenario runs with higher temperatures, the lake ice season in the Nordic area is typically 1–2 months shorter. The largest changes occur in both RCA-H and RCA-E in southern–central Sweden, southwestern Baltic States and western Norway. In these areas, the winters are comparably mild even in the control runs and the simulated ice

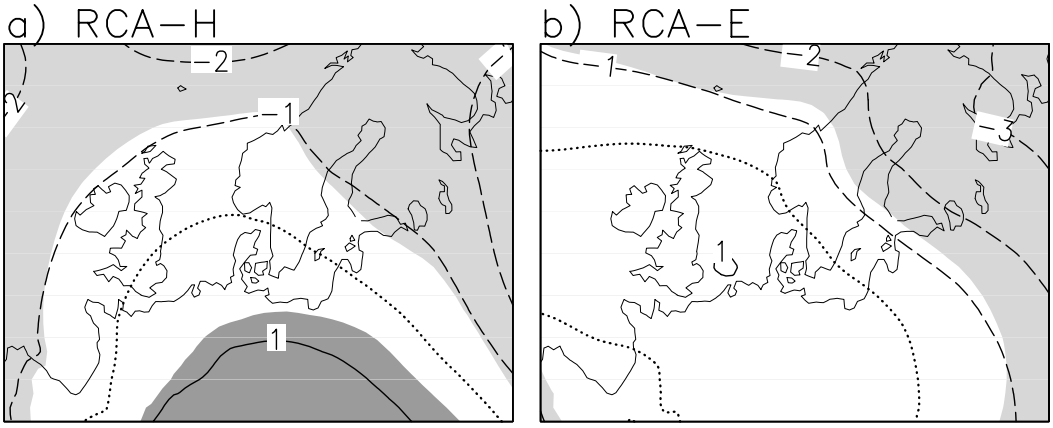

Fig. 8. Changes in annual mean sea level pressure in RCA-H (left) and RCA-E (right). Contours at every 1 hPa; increases (decreases) significant at the 90% level are shaded in dark (light).

conditions are therefore strongly sensitive to changes in temperature. Further northeast, where the control climate is colder, the decrease in ice season length is smaller although the average warming is similar. As expected, the absolute change is also small in areas such as Denmark where the average ice season is very short even in the control runs.

The simulated lake ice seasons shortens from its both ends but in RCA-E, in particular, the change in the date of freezing is in most of the Nordic area larger than the change in the date of melting (Table 4). As averaged over Finland, Sweden and Norway, the ice-covered time is reduced in RCA-E by 26 days in October–January (the typical freezing period) and by 17 days in March–May (the typical melting period). This is consistent with a larger simulated warming in late autumn and early winter than in spring in the same area (the area means for the mentioned two periods in RCA-E are 5.1°C and 2.5°C). In RCA-H, the difference between the changes in freezing and melting dates is smaller, as is the contrast in warming between the two periods (4.1°C and 3.2°C).

The Baltic Sea ice season also shortens substantially in the RCA experiments, in relative terms more so than the lake ice season. The average ice-covered time in the two control runs is in fair agreement with climatological means (Swedish Meteorological and Hydrological Institute and Finnish Institute of Marine Research, 1982), reaching 3–4 months in the northernmost (the Bothnian Bay) and easternmost (the Gulf of Finland) sub-basins. Some undersimulation of ice in the extremes of these two sub-basins, where the ice season in nature is longest, does occur, but this is partly associated with the impossibility of simulating geographical variations within the individual sub-basins in the 1.5-dimensional model (Rummukainen et al., 2000). In the scenario runs, the average ice-covered period only lasts for 50–60 days in the Bay of Bothnia and 20–30 days in the Gulf of Finland. The rest of the Baltic Sea becomes almost ice-free in both RCA-H and RCA-E.

Ice conditions in the Nordic area differ markedly from year to year in nature. For example, the maximum annual Baltic Sea ice extent varied in 1720–1996 from 12% to 100% of a total of 420.000 km^2, with a mean value of about 52% (Tinz, 1996). Similar variation occurs in the RCA simulations (Fig. 10), but around a much lower mean value in the scenario runs than in the control runs. In the control runs, the annual maximum ranges from 33% to 91% in RCA-H and from 11% to 83% in RCA-E, in the scenario runs from 4% to 39% in RCA-H and from 0 to 57% in RCA-E. Thus, although one winter with moderately severe ice conditions occurs in the RCA-E scenario run, both scenario runs also include several winters when the ice extent is below the observed minimum of 12% (there is also one winter marginally below this limit in the RCA-E

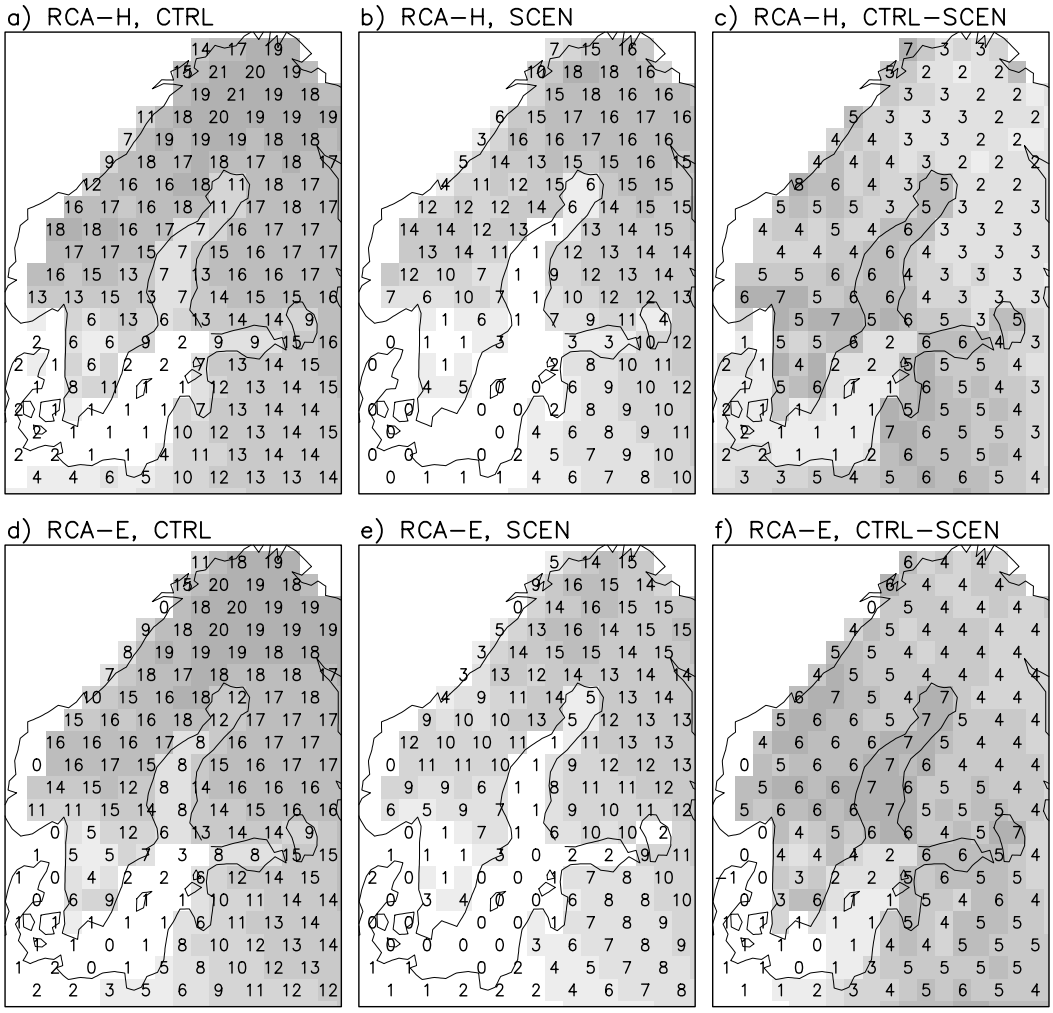

Fig. 9. Average length of the ice season (unit = 10 days) in the Baltic Sea and in inland lakes of northern Europe in the RCA-H and RCA-E control (left) and scenario runs (middle), and the difference control–scenario (right). Numeric values are plotted at every second grid box, excluding the boxes with no ice (0 indicates nonzero values of less than 5 days). The shading increases in darkness with increasing ice season length and with increasing control–scenario difference.

control run). In the RCA-E scenario run, one totally ice-free winter occurs. The decrease in the average annual maximum from the control run to the scenario run is from 53% to 18% in RCA-H, and from 49% to 14% in RCA-E.

Omstedt and Nyberg (1996) studied the sensitivity of the Baltic Sea ice cover to climatic warming using the 1.5-dimensional model in off-line mode. A control run using observed meteorological forcing from 1980–1993 was followed by a run in which the observed atmospheric temperatures were perturbed according to an idealized scenario (2.5°C of warming in summer and 5.5°C in winter). As a result of this prescribed warming, the simulated average annual maximum ice cover was reduced from about 47% (199.000 km^2) to 13% (54.000 km^2). These off-line results are in good agreement with the present on-line simulations,

Table 4. *Average number of days with lake ice in the RCA-H and RCA-E control and scenario runs, and the decrease from the control to the scenario*

	RCA-H			RCA-E		
	Oct–Jan	March–May	Year	Oct–Jan	March–May	Year
control	58	63	149	60	57	145
scenario	39	47	111	34	40	98
decrease	19	16	38	26	17	47

All values are area means over Finland, Sweden and Norway, excluding that part of Norway where the lake model is not applied. Results are shown for the whole year and for the principal freezing (October–January) and melting (March–May) seasons.

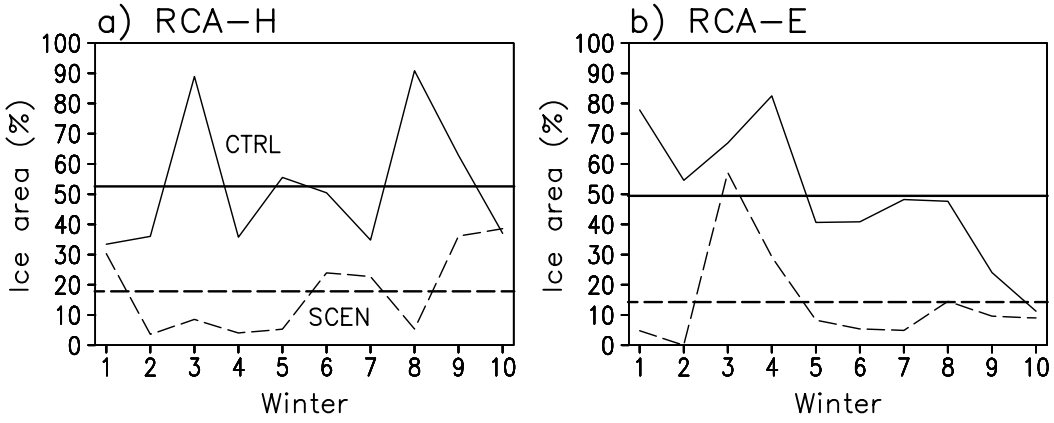

Fig. 10. Annual maximum ice extent in the Baltic Sea (% of a total area of about 420.000 km^2) in (a) RCA-H and (b) RCA-E. The thin solid (dashed) lines show the simulated maximum ice extent in the ten individual control (scenario) run winters and the thick solid and dashed lines the respective 10-year means.

even though in the present simulations a similar reduction in ice is obtained with a slightly smaller warming.

The decrease of sea ice leads, in many GCMs, to a pronounced maximum of wintertime warming over the Arctic Ocean (Kattenberg et al., 1996). How much the local water bodies modify the simulated climate change in the Nordic region in RCA is more difficult to estimate. One indication of the delicate nature of this question is that the contrast in the simulated DJF surface air warming between the northern Baltic Sea and the surrounding land actually differs qualitatively between RCA-H and RCA-E (Fig. 11a, b). In RCA-E, the decrease in ice does induce a local maximum of warming over the Bothnian Bay, but in RCA-H the warming in the same sea area is marginally smaller than over the surrounding land.

The mentioned lack of a maximum in warming in RCA-H and the relative weakness of this maximum in RCA-E are associated with the fact that the Baltic Sea is, even in its northern parts, partly ice-free even in the control runs. Even in late winter, the ice dynamics parameterization in RCA generally precludes the ice cover to reach full 100% (see the lower panels of Fig. 11 for means of ice cover and water temperature in the northern Baltic Sea). The open water makes the wintertime air temperatures over the sea higher than over the surrounding land. However, the increase in water temperature from the control runs to the scenario runs is modest compared with the large warming over land areas. This is partly because the water

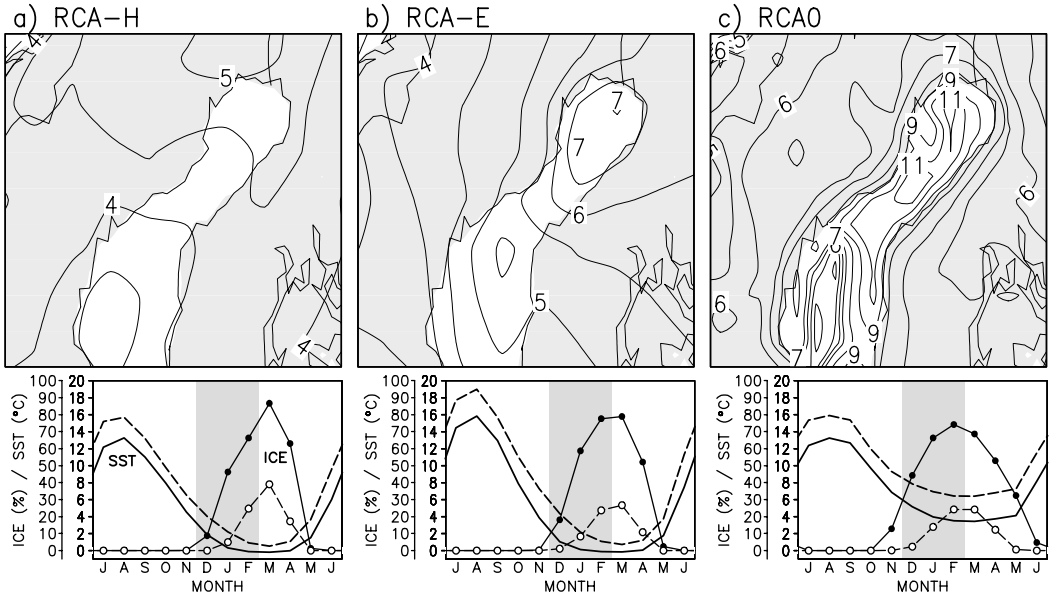

Fig. 11. The change in December–February mean surface air temperature around the northern parts of the Baltic Sea (above) and seasonal cycles of sea surface temperature (lines without markers) and ice cover (lines with markers) averaged over this sea area (below). Results are shown for (a) RCA-H, (b) RCA-E, and (c) RCA0. Contours in the maps at every 0.5°C until 7°C and every 1°C thereafter. In the lower panels, the solid lines represent the control runs and the dashed lines the scenario runs; the December–February period is indicated with shading.

temperature is bounded from below by the freezing point (slightly below 0°C in the northern Baltic Sea which has a surface salinity of about 5‰). To another part, this difference may reflect positive feedbacks associated with snow cover and strong surface layer stability that enhance the warming over the land but not over open water. Thus, although the increase of open water would tend to make, if acting alone, the warming larger over the Baltic Sea than over land, this is counteracted by the relatively small increase in the water temperature. The net effect of these two factors on the land-sea contrast in warming differs between RCA-H and RCA-E probably because RCA-E shows a somewhat larger decrease in December-February ice cover than RCA-H. There is, in this part of the winter, more ice in the RCA-E than in the RCA-H control run, whereas the difference in the scenario run ice cover is small.

Thus, it is not clear whether a physically consistent modelling of the Nordic water bodies amplifies or moderates the simulated atmospheric climate changes. What is more evident is that a bad treatment of these water bodies may create problems. Before the RCA1 simulations discussed in this paper, an earlier version of the Rossby Centre model (RCA0) was applied to simulate climate change using the same HadCM2 boundary data as in RCA-H (Räisänen et al., 1999). In contrast with RCA-H and RCA-E, RCA0 showed a very strong maximum (locally up to 11°C) of wintertime warming over the northern Baltic Sea (Fig. 11c). This questionable feature is associated with a physically inconsistent treatment of the Baltic Sea in RCA0. The water surface temperatures in RCA0 were taken directly from HadCM2, which was problematic since the HadCM2 simulated winter SST in the northern Baltic Sea had a serious warm bias in the control run (a similar problem was associated with the extrapolation of the warm HadCM2 SSTs to inland lakes). To prevent this from deteriorating the control climate, ice cover in the Baltic Sea and in inland lakes was made independent of water temperature and was rather inferred from soil temperatures (Rummukainen et al., 1998). This "ice proxy" model yielded, when suitably tuned, a broadly realistic ice climate in the control run.

The predicted decrease of ice cover from the control run to the scenario run was also fairly similar to the RCA1 results. For simulating changes in air temperature (and some other aspects of surface climate), however, this formulation was a bad choice. The very high water temperatures taken from HadCM2 (in the scenario run in the northern Baltic Sea above 6°C even in late winter; see the lower part of Fig. 11c) made in RCA0 the sensitivity of air temperature to the decrease of ice too large. The warming over the northern Baltic Sea was therefore severely overestimated, at least in comparison with the more self-consistent RCA-H results. Partly as a remote effect of the Baltic Sea changes and partly due to a similarly exaggerated feedback from reduced lake ice, the wintertime warming in RCA0 was 1–2°C larger than in RCA-H even in most of the Nordic land area.

Of the driving global models, neither HadCM2 nor ECHAM4 includes inland lakes, and the Baltic Sea is resolved only marginally. The control run biases in the Baltic Sea SSTs are also generally larger in the GCMs than in RCA (Rummukainen et al., 2000). In the northern Baltic Sea, though, ECHAM4 provides more realistic results than HadCM2, in which the warm winter bias keeps the sea completely ice-free even in the control run time slice. ECHAM4 does have some Baltic Sea ice in the control run, and a majority but not all of this vanishes in the scenario run. This is in qualitative agreement with the RCA results but the crude Baltic Sea geometry in ECHAM4 precludes a more quantitative comparison.

6. Summary and discussion

Two regional climate change experiments have recently been made in one-way nesting mode using version RCA1 of the Rossby Centre regional Atmospheric climate model for northern and central Europe. These two experiments got their boundary data from global greenhouse gas experiments made with two different atmosphere–ocean GCMs, HadCM2 and ECHAM4/OPYC3. Most of the attention here was put on changes in time mean temperature and precipitation, which are probably the two most commonly used indicators of climate change. A quantitative comparison between the two RCA experiments and the two driving GCM experiments yielded the following main findings concerning these variables:

(1) Many aspects of the simulated climate change are reasonably similar between the two RCA experiments. This is the case with, in particular, the overall magnitude of the simulated warming. Common features in the simulated precipitation change include a general increase in annual precipitation in northern Europe.

(2) Sizeable differences in climate change between the two RCA experiments also do occur. On the GCM-resolved scales, these differences are neither systematically smaller nor systematically larger than the differences between HadCM2 and ECHAM4. The root-mean-square difference of the local precipitation changes is, however, larger between the two RCA simulations than between the two GCMs. This reflects the sub-GCM scale details of precipitation change in RCA that vary with the driving GCM simulation.

(3) The temperature and precipitation changes in RCA are strongly governed by the driving GCM simulations. Even on the 88 km grid box scale, the seasonal and annual root-mean-square differences between the changes in RCA and the driving GCM are always smaller than the differences between the two GCM (or the two RCA) experiments themselves. This is the case although the two GCM experiments share virtually the same global mean warming of 2.6°C.

(4) The two RCA experiments both indicate, in most of the model area, a slightly smaller warming than their driving GCM experiments. This appears to be, however, mostly associated with weaknesses in the RCA radiation code rather than with the higher resolution. Other RCM experiments made for Europe show examples of both reduced and increased warming relative to their driving GCMs (Machenhauer et al., 1998). Overall, most of the differences in temperature and precipitation change between RCA and the bilinearly interpolated GCM results occur on scales that are at least formally resolved by the GCMs, rather than on the sub-GCM scale. This complicates the interpretation of these differences.

(5) Internal variability is, because of the shortness of the two RCA experiments, of major importance in interpreting the differences between their results (although not discussed explicitly, this applies to the driving GCM time slices as well).

Typically, about a half of the local RCA–RCA differences in temperature and precipitation change seem to be explainable by this factor, even when neglecting interannual autocorrelation. The differences in precipitation change between RCA and the driving GCMs also appear to be very substantially affected by internal variability.

These results have implications on how regional climate change scenarios should be constructed. Regarding RCM simulations,

(1) Simulation periods longer than 10 years would be desirable to reduce the impact of internal variability. Alternatively, ensembles of 10-year regional simulations could be used, employing boundary data from ensemble GCM experiments with different initial conditions.

(2) The lengthening of the simulations does not remove the need of forcing the RCM with boundary data from different GCMs to capture the uncertainty related to differences between different GCMs in their true noise-free response to increased greenhouse gases.

A third, fundamental implication from the relative smallness of the RCA–GCM differences compared with the inter-GCM differences is that, for impact studies using just changes in time mean temperature and precipitation, downscaling may often be a secondary issue. As far as the purpose of the scenarios is to sample the "probability distribution" of future climate changes, GCMs in fact have the advantage over RCMs that they are global and their results are therefore available, for any given region, in a larger number than RCM results. Of course, the statistics representing the whole RCA model area may underestimate the resolution sensitivity of temperature and precipitation changes in areas of most complex physiography, such as in the immediate vicinity of coastlines and sharp orography. Likewise, a RCM resolution higher than 88 km might to some extent increase the differences from the driving GCM, at least regarding the amplitude of the sub-GCM scale details.

In any event, the main value of regional climate modelling is likely to be in aspects other than just modifying GCM produced estimates of time mean temperature and precipitation change. Some examples of such aspects are listed below:

(1) The existence of sub-GCM scale details in RCM-simulated climate change indicates that climate change in nature will also exhibit such details (even though, in relatively short simulations such as those reported here, the amplitude of these details is likely to be exaggerated by internal variability). In this respect, comparison between different RCM experiments forms a more adequate basis for estimating the uncertainty in local climate change than comparison between GCM experiments in which such details are absent.

(2) The higher resolution in RCMs allows the estimates of climate change to be, on regional scales, more physically consistent between different variables and with the characteristics of the underlaying surface (as discussed in Section 4.5 for the combination of changes in sea level pressure and precipitation in the vicinity of the Scandinavian mountains).

(3) RCMs provide a framework for including in climate change studies components of the regional climate system that are poorly represented or completely absent in current GCMs (Giorgi and Mearns, 1999). In RCA, modules for inland lakes and the Baltic Sea provide physically plausible estimates of how the conditions of these water bodies will change along with changes in the atmospheric climate. Moreover, the interactive coupling allows feedbacks from these water bodies to affect the atmospheric climate change.

(4) More so than with the time mean climate, the high resolution of RCMs might be important in simulating changes in the daily variability of local climate. Some aspects of this, such as the frequency distribution of daily precipitation, have been found quite sensitive to model resolution. This is the case at least regarding the control climate (Jones et al., 1997; Christensen et al., 1998; Murphy, 1999). The findings of Jones et al. (1997) suggest it to be true even for the simulated climate changes, although this may depend partly on how the changes in the frequency distribution are measured.

In conclusion, the relative merits of GCMs and RCMs in producing scenarios of future regional climate still require a lot of research. The capability of RCMs to produce new useful information on time mean temperature and precipitation changes appears to be, because of substantial differences between different GCM simulations, relatively limited. For obtaining useful information on other

aspects of climate change, dynamical downscaling may turn out more important.

7. Acknowledgements

The SWECLIM programme and the Rossby Centre are funded by MISTRA and by SMHI. The HadCM2 data used to drive RCA were provided by the Hadley Centre, and the ECHAM4 data by the Max Planck Institute for Meteorology and the German Climate Computing Centre. The latter data management benefited from cooperation with the Norwegian RegClim project. RCA has been run on the CRAY T3E at the Swedish National Supercomputing Centre (NSC). The Rossby Centre staff members are acknowledged for their efforts in developing the RCA model and conducting the experiments analysed here, and the anonymous reviewers for their constructive comments on an earlier version of this paper.

8. Appendix

Impact of interannual variability on relative precipitation change

Relative precipitation change is defined as

$$\Delta P = \frac{S}{C} - 1, \tag{A1}$$

where C and S denote the control and scenario run mean precipitation. The change in this due to small perturbations δC and δS in the control and scenario run means is

$$\delta(\Delta P) \approx \frac{\partial(\Delta P)}{\partial C}\,\delta C + \frac{\partial(\Delta P)}{\partial S}\,\delta S = -\frac{S}{C^2}\,\delta C + \frac{1}{C}\,\delta S. \tag{A2}$$

Suppose that the noise-free values of C and S are C_0 and S_0, and that the 10-year mean deviations δC and δS have probability distributions with a mean value of zero and variances of VAR(C) and VAR(S). Then, (A2) indicates the variance of ΔP to be, provided that internal variability is weak and uncorrelated between the control and scenario runs

$$V \approx \frac{S_0^2}{C_0^4}\,\mathrm{VAR}(C) + \frac{1}{C_0^2}\,\mathrm{VAR}(S). \tag{A3}$$

From this, (7) is obtained by substituting for C_0 and S_0 the actual 10-year means C and S, and by assuming that individual years are statistically independent and that (A3) is valid even when the variations around C_0 and S_0 are not small.

To test the validity of (7) when interannual variability has a realistic amplitude, synthetic 10-value "control" and "scenario" time series of precipitation were produced with a random number generator. Gaussian distributions with pre-specified means and standard deviations were assumed, except that occasional negative values were replaced with zero. The predictions of variance obtained by substituting the 10-value means and variances to (7) were compared with the actual variances within these large (4×10^5) synthetic ensembles of precipitation change. Results for different values of the noise-free relative change and coefficient of variation a (ratio between the interannual standard deviation and the mean value) are shown in columns 2–4 of Table 5. For the investigated part of the parameter space, (7) gives a good estimate of the actual variance in relative precipitation change. With increasing interannual variation, the variance is slightly overestimated, but even with $a = 0.5$ the overestimate only amounts to about 4% (typical values of a in the RCA simulations are about 0.15 for the annual mean and 0.25–0.45 for seasonal means of precipitation).

For the difference in precipitation change between RCA (subscript 1) and the driving GCM (subscript 2), (A2) is replaced with

$$\delta(\Delta P_1 - \Delta P_2) \approx -\frac{S_1}{C_1^2}\,\delta C_1 + \frac{1}{C_1}\,\delta S_1 + \frac{S_2}{C_2^2}\,\delta C_2 - \frac{1}{C_2}\,\delta S_2. \tag{A4}$$

Taking into account that C_1 and S_1 are not independent from C_2 and S_2 (which makes it inappropriate to sum up the variances of the 4 rhs terms), this gives, at the limit of small perturbations

$$V = \mathrm{VAR}\left(\frac{S_{O_1}}{C_{O_1}^2}\,C_1 - \frac{S_{O_2}}{C_{O_2}^2}\,C_2\right)$$

Table 5. *The ratio between the average estimated and actual variance of 10-year relative precipitation changes in Monte Carlo tests*

	Relative change			Difference in relative change		
change	$a = 0.1$	$a = 0.25$	$a = 0.5$	$a = 0.1$	$a = 0.25$	$a = 0.5$
−50%	1.004	1.012	1.037	1.007	1.022	1.074
0%	1.004	1.012	1.037	1.007	1.022	1.074
50%	1.004	1.012	1.037	1.007	1.022	1.074
50%/25%				1.006	1.021	1.071

Results are shown for the change in a single model (columns 2–4, using (7) to estimate the interdecadal variance from interannual variability) and for the difference in change between two correlated models (columns 5–7, using (8)). The first column gives the noise-free relative change $100\% \times (S/C - 1)$ assumed in creating the time series; in the last case a 50% increase is specified for one and a 25% increase for the other model. The parameter a is the assumed interannual coefficient of variation.

$$+ \mathrm{VAR}\left(\frac{1}{C_{O_1}} S_1 - \frac{1}{C_{O_2}} S_2\right), \tag{A5}$$

which with the assumptions specified above leads to (8). Monte Carlo tests indicate (8) to give a reasonable estimate of the variance of the difference in precipitation change between two models with correlated interannual variations (columns 5–7 of Table 5). The overestimate with large interannual variation is, though, somewhat larger than that obtained from (7) for the one-model case. These results depend slightly on the correlation assumed between the time series in the two models. For Table 5 a characteristic value of 0.8 is used.

As also indicated by Table 5, the relative errors in the estimated variance are for both (7) and (8) independent of the pre-specified noise-free precipitation changes, except that (8) shows a slight sensitivity to differences in the pre-specified change between the two models.

REFERENCES

Christensen, O. B., Christensen, J. H., Machenhauer, B. and Botzet, M. 1998. Very high-resolution regional climate simulations over Scandinavia — present climate. *J. Climate* **11**, 3204–3229.

Eerola, K., Salmond, D., Gustafsson, N., Garcia-Moya, J.-A., Lönnberg, P. and Järvenoja, S. 1997. A parallel version of the HIRLAM forecast model: Strategy and results. In Hoffmann, G.-R. and Kreitz, N. (eds): Making its mark. *Proceedings of the 7th ECMWF Workshop on the use of parallel processors in meteorology*. World Scientific Publishing, Singapore, pp. 134–143.

Giorgi, F. and Mearns, L. O. 1991. Approaches to the simulation of regional climate change: A review. *Rev. Geophys.* **29**, 191–216.

Giorgi, F. and Mearns, L. O. 1999. Introduction to special section: regional climate modeling revisited. *J. Geophys. Res.* **104**, 6335–6352.

Giorgi, F., Marinucci, M. R., Bates, G. T. and De Canio, G. 1993. Development of a second-generation Regional Climate Model (RegCM2). Part II: Convective processes and assimilation of lateral boundary conditions. *Mon. Wea. Rev.* **121**, 2814–2832.

Giorgi, F., Brodeur, C. S. and Bates, G. T. 1994. Regional climate change scenarios over the United States produced with a nested regional climate model. *J. Clim.* **7**, 375–399.

Hulme, M., Conway D., Jones, P. D., Jiang, T., Zhou, X., Barrow, E. M. and Turney, C. 1995. *A 1961–90 gridded surface climatology for Europe*. Climatic Research Unit, Norwich, UK, 51 pp. + maps.

Johns, T. C., Carnell, R. E., Crossley, J. F., Gregory, J. M., Mitchell, J. F. B., Senior, C. A., Tett, S. F. B. and Wood, R. A. 1997. The second Hadley Centre coupled ocean–atmosphere GCM: model description, spinup and validation. *Climate Dynamics* **13**, 103–134.

Jones, R. G., Murphy, J. M. and Noguer, M. 1995. Simulation of climate change over Europe using a nested regional-climate model (I). Assessment of control climate, including sensitivity to location of lateral boundaries. *Quart. J. Roy. Meteor. Soc.* **121**, 1413–1449.

Jones, R. G., Murphy, J. M., Noquer, M. and Keen, A. B. 1997. Simulation of climate change over Europe using a nested regional-climate model (II). Comparison of driving and regional model responses to a doubling of carbon dioxide. *Quart. J. Roy. Meteor. Soc.* **123**, 265–292.

Kattenberg, A., Giorgi, F., Grassl, H., Meehl, G. A.,

Mitchell, J. F. B., Stouffer, R. J., Tokioka, T., Weaver, A. J. and Wigley, T. M. L. 1996. Climate models — projections of future climate. *Climate Change 1995. The science of climate change* (ed. J. T. Houghton, L. G. Meira Filho, B. Callander, N. Harris, A. Kattenberg and K. Maskell). Cambridge University Press, pp. 285–357.

Källén, E. (ed) 1996. *HIRLAM documentation manual.* System 2.5. 178 pp. + 55 pp. appendix. Available from SMHI, S-60176 Norrköping, Sweden.

Ljungemyr, P., Gustafsson, N. and Omstedt, A. 1996. Parameterization of lake thermodynamics in a high resolution weather forecasting model. *Tellus* **48A**, 608–621.

Machenhauer, B., Windelband, M., Botzet, M., Christensen, J. H., Déqué, M., Jones, R. G., Ruti, P. M. and Visconti, G. 1998. *Validation and analysis of regional present-day climate and climate change simulations over Europe.* Max-Planck-Institut für Meteorologie, Report no. 275, Hamburg, Germany, 87 pp. + figures and tables.

McGregor, J. L. 1997. Regional climate modeling. *Meteorol. Atmos. Phys.* **63**, 105–117.

Mitchell, J. F. B. and Johns, T. C. 1997. On modification of global warming by sulphate aerosols. *J. Climate* **10**, 245–267.

Murphy, J. 1999. An evaluation of statistical and dynamical techniques for downscaling local climate. *J. Climate* **12**, 2256–2284.

Noguer, M., Jones, R. and Murphy, J. 1998. Sources of systematic errors in the climatology of a regional climate model over Europe. *Climate Dynamics* **14**, 691–712.

Oberhuber, J. M. 1993. Simulation of the Atlantic circulation with a coupled sea ice-mixed layer-isopycnal general circulation model. Part I: Model description. *J. Phys. Oceanogr.* **22**, 808–829.

Omstedt, A. 1999. Forecasting ice on lakes, estuaries and shelf seas. In: *Ice physics in the natural and endangered environment* (ed: J. S. Wettlaufer, J. G. Dash and N. Untersteiner), NATO ASI Vol. I 56, Springer-Verlag, Berlin, Heidelberg, Germany, pp. 185–208.

Omstedt, A. and Nyberg, L. 1996. Response of Baltic Sea ice to seasonal, interannual forcing and climate change. *Tellus* **48A**, 644–662.

Renwick, J. A., Katzfey, J. J., Nguyen, K. C. and McGregor, J. L. 1998. Regional model simulations of New Zealand climate. *J. Geophys. Res.* **103**, 5973–5982.

Roeckner, E., Arpe, K., Bengtsson, L., Christoph, M., Claussen, M., Dümenil, L., Esch, M., Giorgetta, M., Schlese, U. and Schulzweida, U. 1996. *The atmospheric general circulation model ECHAM-4. Model description and simulation of present-day climate.* Max-Planck-Institut für Meteorologie, Report no. 218, Hamburg, Germany, 90 pp.

Roeckner, E., Bengtsson, L., Feichter, J., Lelieveld, J. and Rodhe, H. 1999. Transient climate change simulations with a coupled atmosphere–ocean GCM including the tropospheric sulfur cycle. *J. Climate* **12**, 3004–3032.

Rummukainen, M., Räisänen, J., Ullerstig, A., Bringfelt, B., Hansson, U., Graham, P. and Willén, U. 1998. RCA — Rossby Centre regional Atmospheric climate model: model description and results from the first multi-year simulation. *Reports Meteorology and Climatology* no. **83**, SMHI, Norrköping, Sweden, 76 pp.

Rummukainen, M., Räisänen, J., Bringfelt, B., Ullerstig, A., Omstedt, A., Willén, U., Hansson, U. and Jones, C. 2000. A regional climate model for northern Europe — model description and results from the downscaling of two GCM control simulations. *Climate Dynamics*, in press.

Räisänen, J., Rummukainen, M., Ullerstig, A., Bringfelt, B., Hansson, U. and Willén, U. 1999. The first Rossby Centre regional climate scenario — dynamical downscaling of CO_2-induced climate change in the HadCM2 GCM. *Reports Meteorology and Climatology* no. **85**. SMHI, Norrköping, Sweden, 56 pp.

Räisänen, P., Rummukainen, M. and Räisänen, J. 2000. *Modification of the HIRLAM radiation scheme for use in the Rossby Centre regional atmospheric climate model.* Report no. **49**, Department of Meteorology, University of Helsinki, Finland, 71 pp

Sass B. H., Rontu, L. and Räisänen, P. 1994. *HIRLAM-2 radiation scheme: documentation and tests.* HIRLAM Technical report no. 16, 43 pp. Available from SMHI, S-60176 Norrköping, Sweden.

Savijärvi, H. 1990. Fast radiation parameterization schemes for mesoscale and short-range forecast models. *J. Appl. Meteor.* **29**, 437–447.

Swedish Meteorological and Hydrological Institute and Finnish Institute of Marine Research, 1982. *Climatological ice atlas for the Baltic Sea, Kattegat, Skagerrak and Lake Vänern (1963–1979).* Sjöfartsverket, Norrköping, Sweden, 220 pp.

Tinz, B. 1996. On the relation between annual maximum extent of ice cover in the Baltic Sea and sea level pressure as well as air temperature field. *Geophysica* **32**, 319–341.